A Generalized Disturbance Filter Design and its Applications to a Spinstand Servo System with Microactuator

Jinchuan Zheng*, Guoxiao Guo†, Youyi Wang‡ and Minyue Fu*
*School of Electrical Engineering and Computer Science
The University of Newcastle, Callaghan, NSW 2308, Australia
Email: Jinchuan.Zheng@newcastle.edu.au
†Data Storage Institute, Singapore 117608
‡School of Electrical & Electronic Engineering
Nanyang Technological University, Singapore 639798

***Abstract*— Narrow-band position error at mid-frequencies around the open-loop crossover frequency can not be effectively reduced using a conventional peak filter, because the attenuation of sensitivity gains has to compromise with the associated decrease of phase margin. This paper presents a general second-order filter that is applicable to reject narrow-band disturbances at any frequency range. The filter zero is designed to minimally degrade the closed-loop system stability and obtain a smooth sensitivity curve around the disturbance frequency. A nonlinear optimization procedure is developed to select the filter parameters such that the statistical position error is minimized. Experimental results of a PZT-actuated head positioning control system on spinstand demonstrate that the add-on filter can further reduce the mid-frequency PES NRRO by 8% and preserve the stability margin of the original control system.**

***Keywords*—Hard disk drive, narrow-band disturbance filter, PZT microactuator, servo control, spinstand.**

I. Introduction

The narrow-band disturbances with spectral energies concentrating at narrow frequency bands commonly exist in a practical servomechanism, e.g., the hard disk drive (HDD) servo system. In HDDs, the track misregistration (TMR) is composed of many factors such as the repeatable runout (RRO) and the nonrepeatable runout (NRRO). Typically, a large portion of the NRRO is contained within narrow frequency bands. In order to meet the requirement for a high track density HDD, the classical loop shaping methods and modern control theories such as H_2 and H_∞ optimal control techniques have been applied to reject the RROs and the narrow-band NRROs [1]. The modern control design based on state-space formulations is an automated design tool, which however often results in an impractically high-order controller. The classical loop shaping methods can provide more intuition and a greater ability to tune designs to achieve performance than the automated tools [2]. The narrow-band disturbance filter proposed in this paper is also based on the classical loop shaping technique.

In the HDD servo, the peak filter was effectively employed to reject the low-frequency (100–600 Hz) narrow-band disturbance caused by disk shift, disk warp and spindle vibration [3]. However, the peak filter is hardly applied to reject the mid-frequency disturbances around the open-loop crossover frequency because of its intrinsic phase loss that negatively impacts the phase margin and distorts the sensitivity gain around the disturbance frequency. Thus, a phase-lead peak filter [4] was proposed to reject the mid-frequency (1.6 kHz) narrow-band disturbances. The filter is improved by adding a differentiator to provide additional $\pi/2$ phase lead such that the phase margin is preserved and the sensitivity curve is smoothly shaped. For the high-frequency (4–10 kHz) narrow-band disturbance rejection, a phase-stabilized servo controller [5] was developed to suppress the windage disturbance caused by suspension vibrations. The controller should be designed to keep the phase of the open-loop system at the disturbance frequency within $-2\pi \pm \pi/2$ and ensure a second phase margin (> 40 deg) to maintain the robust stability.

Previous filter designs are only effective to reject the narrow-band disturbances in a limited frequency range. This paper generalizes the filter design to minimally degrade the closed-loop system stability and effectively reduce the disturbances in an unlimited frequency range by assigning the filter zero. The developed filter was applied to a PZT-actuated head positioning servo system on a spinstand platform. Experimental results demonstrated that the filter can further reduce the mid-frequency position error signal (PES) NRRO by 8%.

II. Generalized Disturbance Filter Realization and Design

This section presents a generalized narrow-band disturbance filter with parallel realization added on a baseline servo system. The design process of the filter parameters is developed such that the resultant servo system can achieve optimal tracking accuracy by rejecting the narrow-band disturbance.

A. Disturbance Filter Structure with Parallel Realization

The disturbance filter structure with parallel realization added on to a baseline servo system is shown in Fig. 1. The

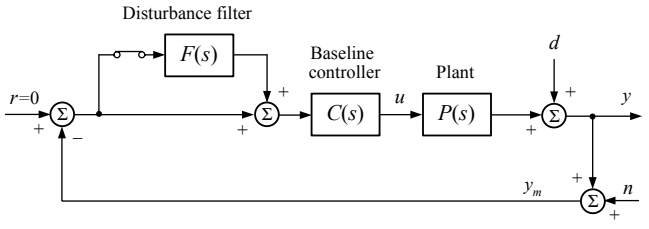

Fig. 1. Block diagram of a disturbance filter structure with parallel realization added on a baseline servo system (y: controlled output; y_m: measured output, d: output disturbance, n: noise).

baseline servo system is assumed to have basic stability and performance. The filter is connected to the baseline controller in a parallel form such that the filter can be easily embedded in the tracking mode. Moreover, the parallel realization has better numerical resolution than cascade realization in the case of fixed-point implementation. The most important advantage for this kind of structure is that the control design can be decoupled into two stages. This can be illustrated by the transfer function from the disturbance d to the controlled output y in Fig. 1, which is given by

$$\begin{aligned} S(s) &= \frac{1}{1+PC(1+F)} \\ &= \frac{1}{1+PC}\frac{1+PC}{1+PC+PCF} \\ &= S_0 S_F \end{aligned} \tag{1}$$

where

$$S_0(s) = \frac{1}{1+PC} \tag{2}$$

$$S_F(s) = \frac{1}{1+T_0F} \tag{3}$$

$$T_0(s) = \frac{PC}{1+PC} \tag{4}$$

Note that S_0 and T_0 are the sensitivity function and complementary sensitivity function of the baseline servo system, respectively. The equation (1) shows that the overall sensitivity function of the closed-loop system is the multiplication of two subsystem S_0 and S_F, which implies that the controllers can be designed by a two-stage approach. In the first stage, we can design the baseline controller $C(s)$ for basic closed-loop stability and disturbance rejection performance indicated by S_0. In the second stage, we can design the filter $F(s)$ based on the pseudo-plant T_0 as shown in (3) such that S_F is shaped to a desired curve for rejecting disturbances in some frequency ranges.

Since we aim at rejecting the narrow-band disturbances, the disturbance filter of the following form can be adopted

$$F(s) = K\frac{s[\omega_0\cos(\varphi) - \sin(\varphi)s]}{s^2 + 2\zeta\omega_0 s + \omega_0^2} \tag{5}$$

where

ω_0: is the disturbance frequency, at which high disturbance rejection is required;

ζ: is the damping ratio with $\zeta \in (0,1)$;

φ: is the phase angle determined by

$$\varphi = \arg\Big[T_0(j\omega_0)\Big] \in [-\pi, \pi] \tag{6}$$

K: is the positive filter gain. Moreover, the closed-loop system will be guaranteed to be stable if

$$0 < K < \gamma \tag{7}$$

where γ is the minimal positive real solution of K in the following two equations

$$\begin{cases} \mathrm{Re}[Q(\omega, K)] = 0 \\ \mathrm{Im}[Q(\omega, K)] = 0 \end{cases} \tag{8}$$

with $Q(\omega, K) = 1 + T_0(j\omega)F(j\omega)$. Here, Re(·) and Im(·) denote the real and imaginary part of a complex number, respectively. Note that if (8) has no solution except $K = \omega = 0$, then $\gamma = +\infty$.

The disturbance filter in (5) is a general high-gain controller structure to reject narrow-band disturbances in a wide frequency range because the filter zero location can be automatically shifted according to the disturbance frequency associated with the baseline servo system. The next two sections will discuss the servo properties of stability and sensitivity gain shaping due to the zero location and the filter gain.

B. Stability Properties Using the Disturbance Filter

The disturbance filter has two complex poles at $p_{1,2} = \omega_0 e^{\pm j\theta}$, where $\theta = \arctan(-\frac{\zeta}{\sqrt{1-\zeta^2}})$. The poles can provide the high loop gain at the disturbance frequency. The filter contains two real zeros at $z_1 = 0$, $z_2 = \omega_0\mathrm{ctan}(\varphi)$. z_1 is specified at the origin in order to maintain the DC gain substantially below the disturbance frequency as that of the baseline servo system such that the corresponding sensitivity gains are not affected. The other zero z_2 is specified in order to achieve phase stabilization, more specifically, the zero will make the departure angles of the filter poles approach to π in the root locus of $T_0(s)F(s)$. This is the correct choice since the poles move in the most stable direction [6]. This property can be verified by Fig. 2. Applying the rule for departure angles from the root locus design method [7], the departure angle from the pole p_1 is given by

$$\phi_{\mathrm{dep}} = \theta + \alpha + \beta - \frac{\pi}{2} + \pi i,\ i = \begin{cases} 1, \text{ for } \varphi \in [-\pi, 0] \\ 0, \text{ for } \varphi \in [0, \pi] \end{cases} \tag{9}$$

where $\alpha = \arg[T_0(p_1)]$ denotes the sum of the angles from the zeros of $T_0(s)$ to p_1 minus the sum of the angles from the poles of $T_0(s)$ to p_1. In practice, the filter damping ratio ζ is chosen as a small value (< 0.1) to provide the high gain at the disturbance frequency. Thus, the filter poles will be very close to the imaginary axis, and we can make the following approximations

$$\theta \approx \frac{\pi}{2} \tag{10}$$

$$\alpha \approx \arg[T_0(j\omega_0)] = \varphi \tag{11}$$

$$\beta \approx \begin{cases} -\varphi, & \text{for } \varphi \in [-\pi, 0] \\ \pi - \varphi, & \text{for } \varphi \in [0, \pi] \end{cases} \tag{12}$$

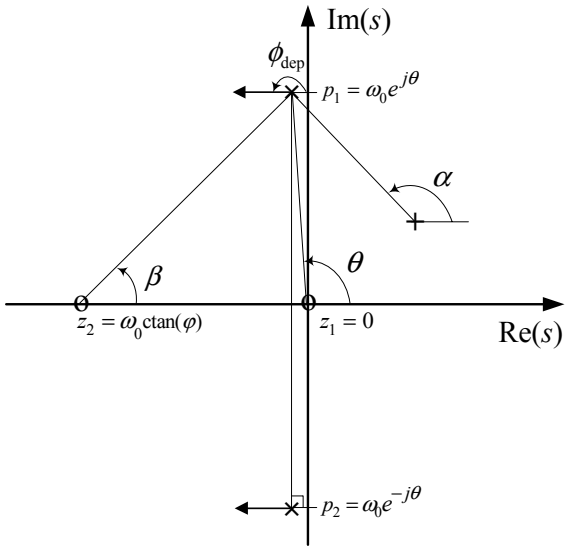

Fig. 2. Root locus for the system $T_0(s)F(s)$. The departure angles from the disturbance filter poles $p_{1,2}$ approach to π by assigning the location of the filter zero z_2.

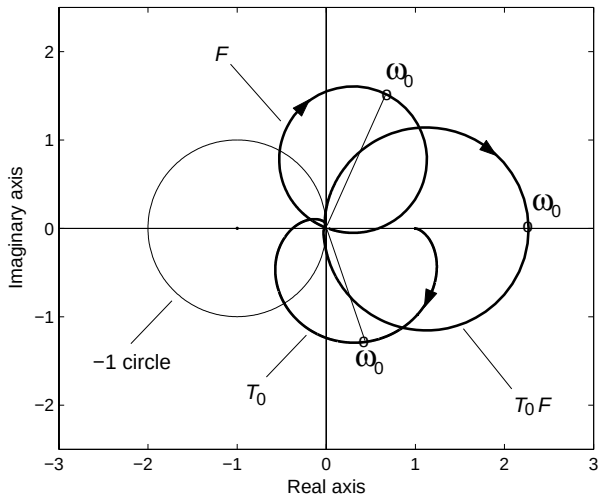

Fig. 3. Nyquist plot. The filter zero provides the exact phase lead such that T_0F at ω_0 is located on the positive real axis. Moreover, the overall curve of T_0F is moved away from the -1 circle, implying reduced sensitivity gains around ω_0 and no obvious distortion of the gains at other frequencies. The "-1 circle" represents the unit circle whose center is at -1 point.

Substituting (10)–(12) into (9), it gives that

$$\phi_{\text{dep}} \approx \pi \tag{13}$$

Therefore, the root locus at the filter poles will move towards the left-half plane (LHP) when the loop gain K increases from 0. The point where the locus crosses the imaginary axis can be computed by (8); and the corresponding K value equals to γ, below which the poles of the closed-loop system are all in the LHP, which guarantees the system stable.

C. Sensitivity Shape Properties Using the Disturbance Filter

The zero placement of the disturbance filter can furthermore lead to another important advantage of minimizing the sensitivity gain at the disturbance frequency without obviously distorting the gains at other frequency bands. This can be confirmed by the sensitivity function of (3), from which it gives that

$$\begin{aligned} |S_F(j\omega_0)| &= \frac{1}{|1 + T_0(j\omega_0)F(j\omega_0)|} \\ &\geq \frac{1}{1 + |T_0(j\omega_0)||F(j\omega_0)|} \end{aligned} \tag{14}$$

By computing the phase angle of $F(s)$ at the disturbance frequency $s = j\omega_0$, it is easy to derive that

$$\arg[T_0(j\omega_0)] + \arg[F(j\omega_0)] = 0 \tag{15}$$

Therefore, the equal mark in (14) holds, which implies that $|S_F(j\omega_0)|$ approaches the minimum value that can be derived as follows

$$|S_F(j\omega_0)|_{\min} = \frac{1}{1 + \frac{K}{2\zeta}|T_0(j\omega_0)|} \tag{16}$$

In fact, the equation (15) indicates that the filter zero provides the exact phase lead amounting to the phase lag of

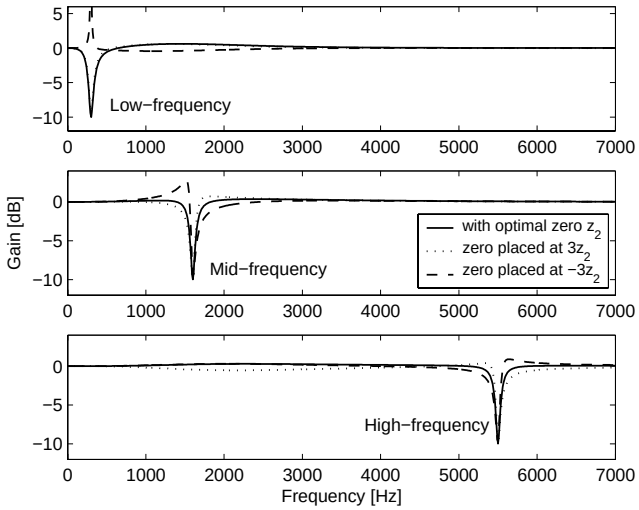

Fig. 4. Frequency responses of the sensitivity gain of $S_F(s)$ with different filter zero placements and disturbance frequency at various frequency range. The curve achieved with optimal zero is smooth without a sharp peak.

$T(s)$ at ω_0 such that the point of $T_0(j\omega_0)F(\omega_0)$ is assured to locate on the positive real axis, where $|S_F(j\omega_0)|$ reaches the minimum. This property can be clearly illustrated from the Nyquist plot in Fig. 3. Another feature observed from the figure is that the phase lead provided by the filter zero tends to move the overall curve of T_0F away from the -1 circle. Thus, the sensitivity gains around ω_0 are reduced, and in the meantime the sensitivity gains at other frequencies are not obviously increased because the curve segments at these frequencies are closed to the neighbourhood of -1 circle. Fig. 4 further shows the comparison of the sensitivity gains obtained with different filter zero placements at various frequency ranges. It is obvious that the filter with optimal zero design achieves a smooth

sensitivity curve around the disturbance frequency, at which the other two filters with different zeros exhibit sharp peaks.

D. Optimal Rejection of the Narrow-Band Disturbance

According to the waterbed effect in linear systems, the push-down sensitivity gains around the narrow-band disturbance frequency is generally accompanied with the pop-up sensitivity gains somewhere else. This phenomenon can be observed from Fig. 4, where the curve achieved by the proposed filter has no sharp peak but still has some region about 0 dB. Therefore, it is necessary to determine the peak value and bandwidth of the filter associated with K and ζ such that the disturbances along the entire frequency band is statistically minimized while maintaining the other performance such as the stability margin and servo bandwidth.

The selection for the disturbance filter parameters K and ζ can be determined by an optimization process based on a MATLAB/Simulink[1] model with the block diagram in Fig. 1. It is assumed that the plant model $P(s)$, the baseline controller $C(s)$ and the disturbance source d are known and the measurement noise n is white noise. In the case that the disturbance is unmeasurable, the method proposed by [8] can be employed to estimate the equivalent disturbance. The method can be simply described as: collect the time traces of the measured output under the baseline servo, say $y_m(k)$, $k = 1, \cdots, N$, where N represents a sufficiently large number of measurement points (e.g., $N = 20000$); then the disturbance time traces can be estimated from the following equation

$$d(k) = Z^{-1}\{S_0(z)^{-1} y_m(z)\} - n(k) \tag{17}$$

where $Z^{-1}\{\bullet\}$ denotes the inverse z transform of a signal; and $n(k)$ has the same PSD (power spectral density) magnitude as the baseline PSD magnitude of $y_m(k)$.

When the disturbance time traces are available, it is easy to obtain the corresponding frequency spectrum plot. Hence, from the plot the disturbance frequency ω_0 of the dominant narrow-band disturbance can be read out directly where the magnitude is relatively high. Alternatively, adaptive technique [9] can be used to search for the dominant disturbance frequency. The disturbance is then injected into the Simulink model and the controlled output $y(k)$ are regenerated for different filter parameters. Finally, the simulated results are evaluated according to the performance criteria such that the optimal filter parameters are determined. Our objective is to minimize the standard deviation of $y(k)$ under the disturbance $d(k)$. Thus, the optimization problem of the filter parameters is formulated as follows

$$\min_{x=(K,\zeta)} \sigma[y(x)] \tag{18}$$

$$\begin{aligned} &\text{subject to the constraints :} \\ &\mathrm{PM}(x) \geq \mathrm{PM}_0 \\ &\mathrm{GM}(x) \geq \mathrm{GM}_0 \\ &f_c(x) \geq f_{c0} \\ &(0,0) \leq x \leq (\gamma, 1) \end{aligned}$$

[1]MATLAB and Simulink are registered trademarks of The Mathworks, Inc.

where PM_0, GM_0 and f_{c0} are the minimal requirements of phase margin (PM), gain margin (GM) and open-loop crossover frequency, respectively; and γ can be determined by (8) for each fixed ζ.

The optimization problem can be solved by using the constrained minimization function *fmincon* in the MATLAB Optimization Toolbox [10]. The following remarks are in order:

(1) The disturbance filter generally causes multiple open-loop crossover frequencies, which leads to multiple candidate PM values. Since the phase margin requires the least phase perturbation to drive the system to instability, we must choose the minimum of all the possible PMs [7]. Therefore, the PM along with the open-loop crossover frequency need to be reevaluated.

(2) A tighten constraints and bound of the variables can help to achieve global minimization. Moreover, a good starting guesses of the variables can improve the execution efficiency and help to locate the global minimum instead of a local minimum. An initial estimate of the filter parameters can be set as

$$\zeta = \frac{\Delta(\omega_0 + 0.5\Delta)}{4\omega_0^2} \tag{19a}$$

$$K = (10^{M/20} - 1)\frac{2\zeta}{|T_0(j\omega_0)|} \tag{19b}$$

where Δ is the disturbance bandwidth, which is defined as the frequency difference between the first two points away from the peak whose magnitudes are $1/\sqrt{2}$ times of the peak value in the frequency spectra plot, and M (unit: dB) is the desired reduction ratio of the narrow-band disturbance.

(3) The solution might be trivial when the narrow-band disturbance is not the dominant disturbance factor on the controlled output.

III. Application

In this section, the disturbance filter design method is applied to a PZT-actuated head positioning control system on a spinstand platform for improved tracking accuracy by rejecting the mid-frequency NRROs.

A. System Description

In disk drive industry, the spinstands are used for the testing and evaluation of magnetic media and heads before the components are assembled into the disk drive during production. With the increasing requirement of a high areal density HDD, it is urgent to increase the track density. Therefore, high precision and efficient servomechanism is needed to position the head on the desired track to support the increased demand for high track density under the spinstand platform. Moreover, precise positioning capability are required for disk media and head testing, track profile and track interference analysis.

We have upgraded the capability of a Guzik spinstand (1701A) with the new design of a PZT head cartridge base [11], which has a displacement range of 2 μm and resolution

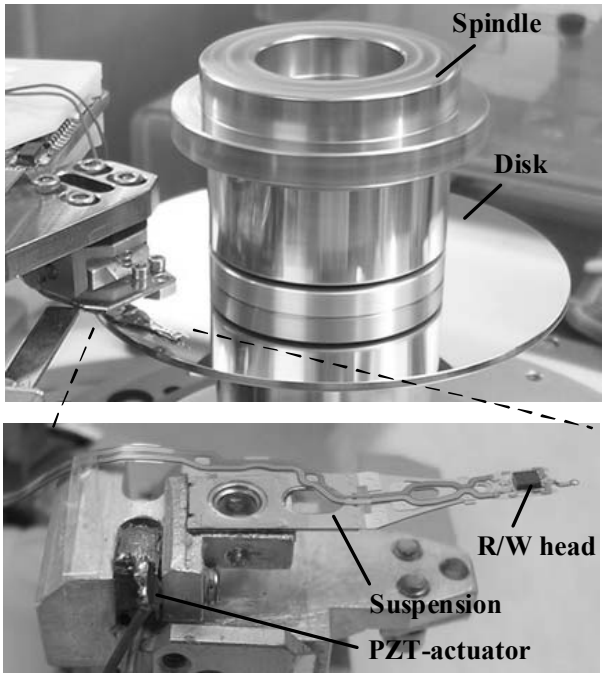

Fig. 5. A PZT-actuated head positioning device on spinstand.

of 0.02 nm as the positioning device for quick and precise tracking purpose. A picture of the platform setup is shown in Fig. 5. The disk is rotated by the spindle at 4000 RPM. The head position servo patterns are prewritten on the disk using a multi-frequency servo encoding and decoding scheme [12]. A dual-frequency PES demodulator implemented within a digitizer board with on-board FPGA (Acqiris AC240) is used to generate the PES based on the readback signals of the servo patterns on real-time with the sampling frequency of 40 kHz. The PES is then fed back to the controller for reader servo control.

The plant model, i.e., the controlled object on the spinstand platform consists of the PZT microactuator, the head cartridge base and a suspension carrying the read/write head. The control input is applied to the PZT microactuator via a PZT amplifier. The control variable PES is the relative error between the head position and the servo sectors prewritten on the disk surface. Here, the plant model $P(s)$ is identified using the following equation with the mechanical system model $P_m(s)$ and the equivalent time delay model $P_d(s)$

$$P(s) = P_m(s)P_d(s) \tag{20a}$$

$$P_m(s) = k\sum_{i=1}^{3}\frac{r_i}{s^2+2\zeta_i\omega_i s+\omega_i^2} \tag{20b}$$

$$P_d(s) = \frac{1}{\frac{T}{2}s+1}e^{-\lambda s} \tag{20c}$$

The modal parameters of the first resonance mode are $r_1 = 1$, $\zeta_1 = 0.015$, and $\omega_1 = 11.5$ kHz. $P_d(s)$ includes an approximate transfer function of the zero-order hold [7] with $T = 25$ μs and a time delay term due to process and computation delay

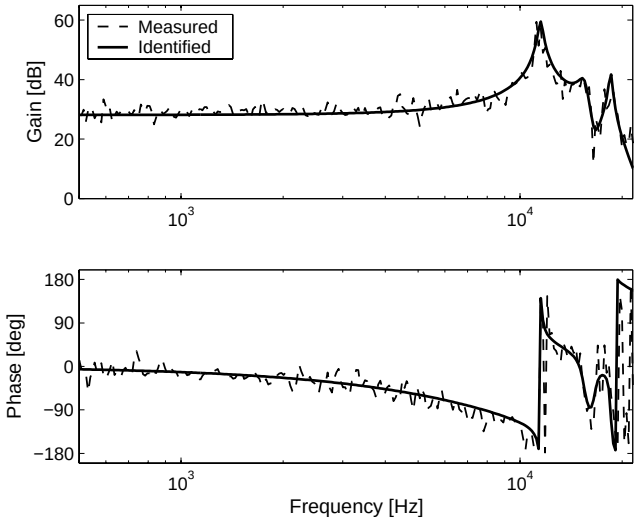

Fig. 6. Frequency responses from PZT amplifier input to PES.

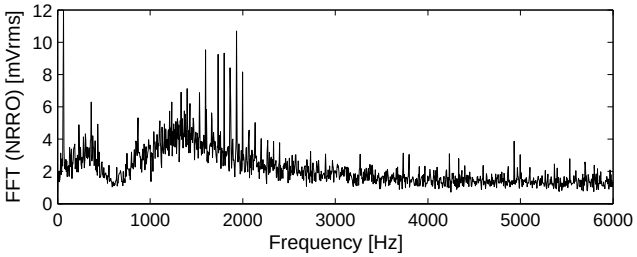

Fig. 7. Frequency spectrum of the PES NRRO with baseline servo (3σ=0.121 μinch).

with $\lambda = 20$ μs. The frequency responses of the identified and measured plant model are shown in Fig. 6.

B. Baseline Servo Design

The baseline controller $C(s)$ is designed such that the servo system ensures the basic stability margin and disturbance and noise rejection performance. The designed $C(s)$ is of the following equation

$$C_s(s) = 0.003\frac{s+2\pi 13000}{s}\cdot\frac{s^2+2890s+(2\pi 11500)^2}{s^2+130100s+(2\pi 11500)^2} \cdot\frac{s^2+6032s+(2\pi 600)^2}{s^2+603.2s+(2\pi 600)^2} \tag{21}$$

which includes a PI controller, a notch filter to gain-stabilize the first resonance mode and a peak filter to suppress the low-frequency (600 Hz) disturbances caused by disk flutter and spindle vibrations. The baseline servo system achieves an open-loop crossover frequency $f_c = 1400$ Hz, GM $= 10$ dB, PM $= 45$ deg (see Fig. 8) and desired disturbance rejection at low frequencies (see Fig. 9). The frequency spectrum of the PES NRRO with baseline servo is shown in Fig. 7.

C. Optimal Filter for Mid-Frequency NRRO Rejection

Fig. 7 indicates that a narrow-band mid-frequency NRRO occurs at the center frequency 1300 Hz, at which the baseline

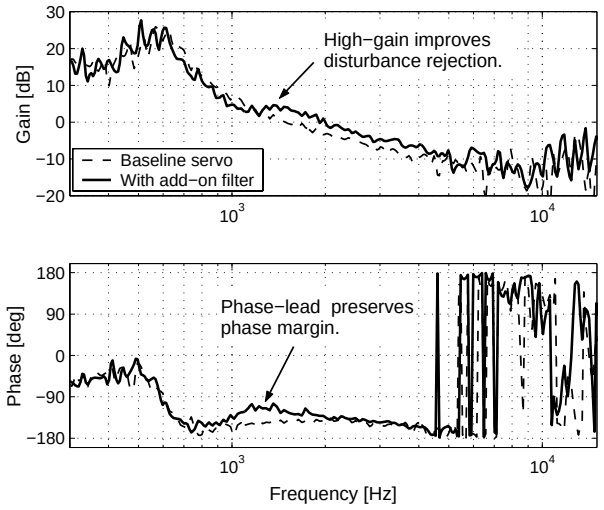

Fig. 8. Measured frequency responses of the open-loop system.

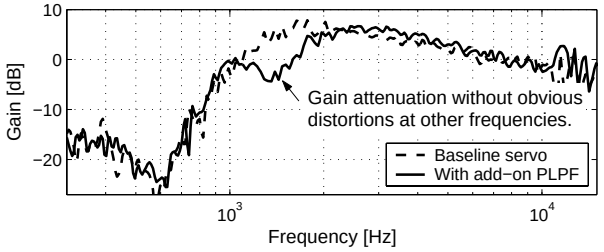

Fig. 9. Measured frequency responses of the sensitivity function.

servo amplifies the disturbances. It is expected that the rejection of the disturbance at this band by the add-on disturbance filter can further reduce the NRRO. Hence, the disturbance filter in (5) has the following directly determined parameters

$$\omega_0 = 2\pi 1300, \quad \varphi = -71 \text{ deg} \tag{22}$$

After carrying out the optimization procedure in Sec. II-D with the constraints chosen as $\text{PM}_0 = 40$ deg, $\text{GM}_0 = 6$ dB, $f_{c0} = 1300$ Hz, the other filter parameters in (5) are obtained as

$$K = 0.26, \quad \zeta = 0.11 \tag{23}$$

The resulting servo system with the add-on filter has the crossover frequency $f_c = 1800$ Hz, GM$= 7$ dB, PM $= 50$ deg. The measured frequency responses in Figs. 8 and 9 show that the add-on filter achieves gain attenuation around 1300 Hz without obviously distorting the shape at other frequencies on the sensitivity curve, while the phase lead feature has preserved the stability margin.

The frequency spectrum of the PES NRRO with the add-on filter is shown in Fig. 10, which indicates that the mid-frequency NRROs around 1300 Hz are significantly attenuated while the NRROs at other frequency bands are not obviously amplified. The PES NRRO 3σ value is further reduced from 0.121 μinch with the baseline servo to 0.111 μinch with the add-on filter, which is a 8% reduction ratio. The improvement can increase the track density from 275 kTPI to 300 kTPI.

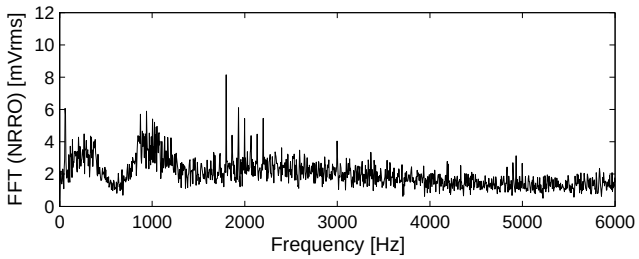

Fig. 10. Frequency spectrum of the PES NRRO with the add-on filter (3σ=0.111 μinch).

IV. Conclusion

A generalized optimal disturbance filter design method is developed to reject the narrow-band disturbances at any frequency range. The filter zero is assigned to minimally degrade the closed-loop system stability and obtain a smooth sensitivity curve around the disturbance frequency. The disturbance filter was applied to a PZT-actuated head positioning servo system on the spinstand platform. Experimental results showed that the add-on filter further reduced the overall 3σ value of PES NRRO by 8% and preserved the stability margin of the original baseline servo system.

Acknowledgment

The authors would like to thank Ms. Wai Ee Wong of Data Storage Institute, Singapore for the valuable help of setting up the experiment platform.

References

[1] T. Yamaguchi, "Modelling and control of a disk file head-positioning system," *Proc. Institution of Mechanical Engineer Part I Journal of Systems and Control Engineering*, vol. 215, pp. 549-567, Dec. 2001.

[2] W. Messner, "Some advances in loop shaping controller design with applications to disk drives," *IEEE Trans. Magn.*, vol. 37, no. 2, pp. 651-656, Mar. 2001.

[3] S. M. Sri-Jayantha, H. Dang, A. Sharma, I. Yoneda, N. Kitazaki and S. Yamamoto, "TrueTrack^{TM} servo technology for high TPI disk drives," *IEEE Trans. Magn.*, vol. 37, no. 2, pp. 871-876, Mar. 2001.

[4] J. Zheng, G. Guo and Y. Wang, "Identification and decentralized control of a dual-actuator hard disk drive system," *IEEE Trans. Magn.*, vol 41, no. 9, pp. 2515-2521, Sep. 2005.

[5] M. Kobayashi, S. Nakagawa and S. Nakamura, "A phase-stabilized servo controller for dual-stage actuators in hard disk drives," *IEEE Trans. Magn.*, vol. 39, no. 2, pp. 844-850, Mar. 2003.

[6] L. A. Sievers and A. Flotow, "Comparison and extensions of control methods for narrow-band disturbance rejection," *IEEE Trans. Signal Processing*, vol. 40, no. 10, pp. 2377-2391, Oct. 1992.

[7] G. F. Franklin, J. D. Powell and A. Emami-Naeini, *Feedback Control of Dynamic Systems*, 3rd ed., Reading, MA: Addison-Wesley, 1994.

[8] H. Lee, "Controller optimization for minimum position error signals of hard disk drives," *IEEE Trans. Magn.*, vol. 48, no. 5, pp. 945-950, Oct. 2001.

[9] Y. Kim, C. Kang and M. Tomizuka, "Adaptive and optimal rejection of non-repeatable disturbance in hard disk drives," in *Proc. IEEE/ASME Int. Conf. on Advanced Intelligent Mechatronics*, 2005, pp. 1-6.

[10] T. Coleman, M. Brace and A. Grace, *Optimization Toolbox for Use with MATLAB*: MathWorks, 1999.

[11] Z. He, G. Guo, L. Feng and W. E. Wong, "A micro actuation mechanism with piezoelectric element for magnetic recording head positioning for spin stand," submitted to *Journal of Mechanical Engineering Science*.

[12] W. E. Wong, L. Feng, G. Guo, W. Ye and A. Al-Mamun, "Implementation of a servo positioning system on spin stand," in *Proc. IEEE Conf. Industrial Electronics*, 2003, vol. 3, pp. 2114-2119.